RSC Advances

PAPER

View Article Online
View Journal | View Issue

Check for updates

Cite this: *RSC Adv.*, 2023, **13**, 6793

In vitro hemocompatibility studies on small-caliber stents for cardiovascular applications

Arumugam Marimuthu,[a] Mahendran Logesh,[a] Khalil El Mabrouk [b] and Anbalagan M. Ballamurugan *[a]

The doping of biologically meaningful ions into biphasic calcium phosphate (BCP) bioceramics, which exhibit biocompatibility with human body parts, has led to their effective use in biomedical applications in recent years. Doping with metal ions while changing the characteristics of the dopant ions, an arrangement of various ions in the Ca/P crystal structure. In our work, small-diameter vascular stents based on BCP and biologically appropriate ion substitute-BCP bioceramic materials were developed for cardiovascular applications. The small-diameter vascular stents were created using an extrusion process. FTIR, XRD, and FESEM were used to identify the functional groups, crystallinity, and morphology of the synthesized bioceramic materials. In addition, investigation of the blood compatibility of the 3D porous vascular stents was carried out *via* hemolysis. The outcomes indicate that the prepared grafts are appropriate for clinical requirements.

Received 29th October 2022
Accepted 8th February 2023

DOI: 10.1039/d2ra06831a

rsc.li/rsc-advances

Open Access Article. Published on 27 February 2023. Downloaded on 4/25/2026 11:50:07 AM.
This article is licensed under a Creative Commons Attribution-NonCommercial 3.0 Unported Licence.

Introduction

Arteries are important soft tissues in humans and animals for the transport of blood cells, nutrients, minerals, oxygen, waste, and other components.[1–3] Injured blood vessels are caused by trauma, narrowing, heart failure, locked blood flow and inadequate nutrient and oxygen supply, and lead to increased risk of mortality and morbidity worldwide.[2,4,5] The foremost therapeutic modalities include pharmacological therapy, interventional therapy, and surgery. In the surgical modality, vascular transplantation is required when the local arteries are severely damaged, unable to ensure regular blood flow, and inappropriate candidates for pharmacological therapy or endovascular therapy.[1,6–9]

A damaged or blocked vessel can be replaced or bypassed using an artificial vascular graft. Recently, clinical autologous bypass therapies have been conducted to construct a new trajectory around the occlusion. However, the procedure can cause side effects such as chills, flushing in the face, lack of taste in the mouth, nausea, vomiting, headache, changes in blood pressure, and breathing problems.[10–12] Additionally, adequate autologous grafts are frequently not accessible due to previous harvesting or the patient's condition. Hence, the development of artificial stents is essential for artery implantations. An increasing number of researchers and businesses have investigated and developed various materials and techniques to create artificial stents *in vitro*.

To develop artificial blood vessels and arteries, numerous synthetic and natural polymers, as well as metals that serve as biomaterials, are being extensively explored and created. Biomaterials include polymers, bioceramics, and metals used for the treatment of bones and dental issues, and for the replacement of damaged blood vessels and arteries.[13–16] There are several traditional metallic messes and coated messes that are used in currently available stents. Even though surface modification is necessary because biological reactions occur immediately after an implant is placed in the body, the material surface has a significant impact on the interactions with the biological environment or leaching of ions in artificial devices. Some researchers have reported the application of bioceramics as coatings with the purpose of expanding the applications and enhancing the functionality and reliability of current biomedical implants. Currently, metal-based stents without coating and ceramic-coated stents are used for the treatment of cardiovascular diseases.[17–23] However, their design and production still make it difficult to achieve the desired availability and product quality.

Calcium phosphate (CaP) has biocompatible properties and is used in a variety of sectors, including biology, biomedical diagnostics, tissue engineering, dental implants, drug delivery, biosensors, MRI contrast agents, blood compatibility and hyperthermia-based treatments. Bioceramic materials have frequently been employed in previous publications for hard tissue repair or as coatings on metallic implants for orthopedics and dentistry.[24–28] The development of bioceramic-material-based stents is a relatively new approach for cardiovascular

[a]*Department of Nanoscience and Technology, Bharathiar University, Coimbatore-641046, India. E-mail: balamurugan@buc.edu.in*

[b]*Euromed Engineering Faculty, Euromed Research Center, Euromed University of Fes, Eco-Campus, Campus UEMF, Fes, Morocco*

© 2023 The Author(s). Published by the Royal Society of Chemistry

Open Access Article. Published on 27 February 2023. Downloaded on 4/25/2026 11:50:07 AM. This article is licensed under a Creative Commons Attribution-NonCommercial 3.0 Unported Licence.

applications. The current report deals with the development of bioceramic cardiovascular stents and their physical, chemical, electrical, and biological properties. Since the bioceramic stents for clinical use is relatively a new approach in the fabrication of vascular grafts.

Materials and methods

Calcium nitrate tetrahydrate ($Ca(NO_3)_2 \cdot 4H_2O$) (Merck, India), magnesium nitrate hexahydrate ($Ni(NO_3)_2 \cdot 6H_2O$) (Merck, India), di-ammonium hydrogen orthophosphate ($(NH_4)_2HPO_4$) (SD Fine Chem, India), ammonia solution (NH_3, above-25%) (Merck, India), polyvinyl alcohol (PVA, Merck, India), 1,6-hexanediol (SD Fine Chem, India), polyethylene glycol (PEG, Nice, India), ammonium persulfate ((APS) ($(NH_4)_2S_2O_8$)), polyvinyl alcohol (PVA), *N*,*N*,*N*′,*N*′-tetramethylethylenediamine (TEMED), and di-functional *N*,*N*′-methylenebisacrylamide ((MBAM) $(C_2H_3CONH)_2CH_2$).

Synthesis of BCP

Biologically relevant ion substituted biphasic calcium phosphate was synthesized *via* a wet chemical precipitation technique. Calcium deficient biphasic calcium phosphates are a large group of materials in which the Ca/P stoichiometry ratio is equal to 1.67. The selected number of moles of di-ammonium hydrogen orthophosphate was dissolved in a 500 mL beaker and the clear supernatant phosphate solution was added dropwise into a 1000 mL RB flask containing the selected number of moles of calcium nitrate and magnesium nitrate solution, and the suspension was maintained under stirring conditions. The initial pH was 4.7, but the required basic pH of near 10 was achieved by adjusting the pH using 25% ammonia solution. A white colloidal precipitate was formed, and a fitted refluxed condenser maintained the temperature at 90 ± 5 °C overnight. Finally, the clear supernatant solution was left undisturbed for settling of the precipitate, and the process was repeated multiple times. The obtained solid was filtered and dried in a hot-air oven at 110 °C. The magnesium-ion-doped BCP cakes were ground and then ball-milled for 48 h at 350 rpm. The ball-milled powder sample was heat-treated at 950 °C for 7 h.

Fabrication of bioceramic (BCP and BCP/Mg-BCP) vascular stents by extrusion technique

The bioceramic stents were produced using an extrusion technique (Fig. 1). The following precursors were used to fabricate vascular grafts: organic monomers – ammonium persulfate as a initiator ((APS) ($(NH_4)_2S_2O_8$)), polyvinyl alcohol (PVA) as a binding agent, *N*,*N*,*N*′,*N*′-tetramethylethylenediamine (TEMED) as a catalyst, di-functional *N*,*N*′-methylenebisacrylamide as a crosslinking agent ((MBAM) $(C_2H_3CONH)_2CH_2$), and bioceramic powder solids (Mg-BCP). All the above-mentioned chemical reagents were mixed to form the bioceramic suspension. A split-type extrusion mould with dimensions of 60 × 30 × 30 mm was used to cast the homogenous precursor suspension that had been prepared. The small-caliber stent fabrication method was previously published in one of our research articles.[29]

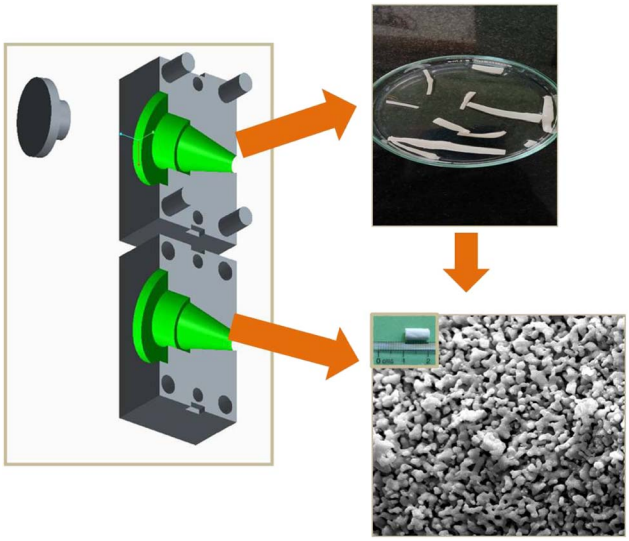

Fig. 1 Extrusion technique for the developed bioceramic-based small-caliber stent.

The extruded small-caliber stents were dried at room temperature and sintered at 950 °C for 24 h using a slow heating rate to avoid shrinkage; the heat treatment process also helped to remove the organic monomers.

Electrochemical impedance analysis

The electrical resistance of the developed vascular stent was measured using a biologic SP300 potentiostat. Electrochemical impedance spectroscopy (EIS) was used to characterize the resistances that develop at the interphases of the bioceramic stent (10 mm length) in intravenous fluid of 0.45% and 0.9% saline electrolytes; the associated Nyquist plots are presented in Fig. 6. To reveal the underlying physical processes, the EIS data were plotted using an equivalent electrical circuit, as shown in the inset of Fig. 6. The frequency range was from 1 MHz to 1 Hz. The resulting impedance occurring at the surface of the material with the NaCl electrolytes was measured. Ag/AgCl and platinum were used as the reference electrode and the auxiliary electrode for the electrochemical cell.

Hemocompatibility

Collection of blood sample. Fresh human blood samples of 5 mL were drawn from healthy volunteers and placed in a 20 mL centrifuge vial together with an anticoagulant agent (2% EDTA) and phosphate buffer saline (PBS) (in accordance with the Indian Council for Medical Research's (ICMR) "National Ethical Guidelines for Biomedical and Health Research Involving Human Participants", Guidelines 2017). The collected human blood samples were diluted in a buffer solution and fresh blood (1 : 4 ratio) and centrifuged for 5 minutes at 6000 rpm to separate the red blood cells (RBC) at room temperature; the supernatant was discarded. The procedure was repeated a few times to completely remove the remaining components. After the extracted RBC were diluted using phosphate buffer saline, 1 μL of red

© 2023 The Author(s). Published by the Royal Society of Chemistry

Open Access Article. Published on 27 February 2023. Downloaded on 4/25/2026 11:50:07 AM.
This article is licensed under a Creative Commons Attribution-NonCommercial 3.0 Unported Licence.

blood cells was added to the desired amount (5 mg, 10 mg, 15 mg, 20 mg, and 25 mg) of the corresponding samples of the bioceramic materials (BCP, 3%Mg/BCP, 7%Mg/BCP, and 10% Mg/BCP) in a 1.5 mL centrifuge vial. The sample tubes were incubated 37 °C for 4 h and centrifuged for 15 min after completion of the 4 h incubation period. After centrifugation, the absorbance of the supernatant buffer solution was measured using a spectrophotometer to quantify the hemolytic activity of the developed bioceramic vascular grafts, and the absorbance at 550 nm was noted. The procedure was executed in triplicate and the results were reported as a percentage considering 50% as the hemolytic concentration for erythrocytes, and the positive control as 100% hemolysis.[30] The obtained values were used to calculate the hemolysis percentage using following equation:

$$\mathrm{HR} = \frac{\mathrm{OD_{Abs}} - \mathrm{OD_{-ve}}}{\mathrm{OD_{+ve}} - \mathrm{OD_{-ve}}} \times 100$$

where $\mathrm{OD_{Abs}}$ is the absorbance of the samples with RBCs, and $\mathrm{OD_{+ve}}$ and $\mathrm{OD_{-ve}}$ are the absorbance of the positive control and negative control, respectively.

Statistical analysis

All data were statistically analyzed with the aid of SPSS Statistics using the one-way analysis of variance (ANOVA) and Tukey's HSD tests (version 16, IBM Corporation, NY). The significance level was set at ≤ 0.01 using the p value. The statistics are displayed as mean and standard deviation (SD). Unless otherwise specified, the same conditions and three appropriate duplicates of the biological studies were carried out for each treatment.[31]

Characterizations

X-ray diffraction analysis (XRD; Bruker AXSD-8) was used to determine the phase behaviour of the samples (BCP, 3%Mg-BCP, 7%Mg-BCP, and 10%Mg-BCP) using monochromatic Cu K radiation at 1.5406 Å. Data were obtained over two θ ranges of 10–80° at a scan rate of 10° $\mathrm{min^{-1}}$. The reported functional groups were recorded using FTIR spectral analysis and the KBr pellet technique on a JASCO-4600 instrument. The morphology of the created small-caliber vascular stents was characterized using FESEM analysis. The electrical impedance was measured using a biologic SP 300 potentiostat.

Results and discussion

X-ray diffractometry (XRD) analysis

Fig. 2 shows the XRD patterns of the prepared calcium deficient biphasic calcium phosphate and calcium deficient biphasic calcium phosphate. The obtained diffraction peaks matched very well with the standard JCPDS pdf files. The XRD patterns show the phase transition of the HAp and β-TCP crystalline phases for Mg^{2+}-ion doped BCP powder. Fig. 2(b)–(d) shows that the obtained crystalline peak intensity of β-TCP increased with increasing the percentages of the doped ion, as well as a decrease in the HAp crystalline phases due to the impact of the magnesium ion. The obtained characteristic peaks of biphasic calcium phosphate (HAp and β-TCP) were indexed according to the standard JCPDS sheets 09-0432 (HAp) and 09-0169 (β-TCP). The corresponding 2θ values and reflection planes of the binary mixture were mentioned in our previous publication.[29,32] The XRD data did not indicate any other impurities of calcium phosphate and confirmed that the synthesized powder samples were biphasic calcium phosphate.

FTIR analysis

The Fourier transform infrared spectroscopy technique was used to identify the functional groups in the metal ion (Mg^{2+})-doped biphasic calcium phosphate sintered at 950 °C. Fig. 3 shows the FTIR spectra, which presented functional groups such as OH^-, H_2O, HPO_4^{2-}, PO_4^{3-}, and CO_3^{2-}. The characteristic absorption bands appeared at the respective absorption wavenumbers (471, 602, 567, 952, 1032, and 1093 $\mathrm{cm^{-1}}$) for the

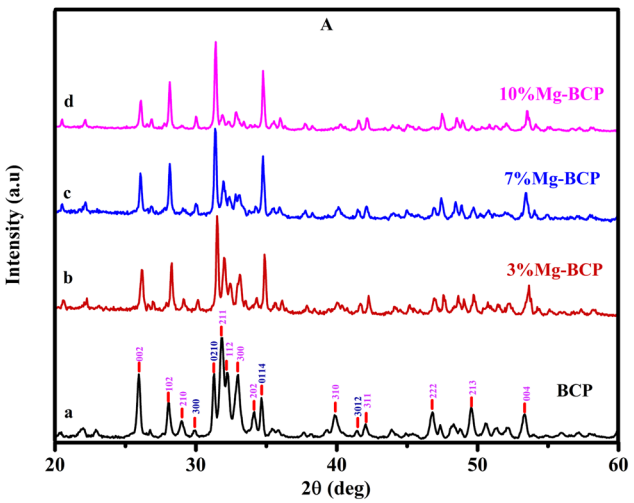

Fig. 2 XRD patterns for pure BCP, 3%Mg-BCP, 7%Mg-BCP, and 10% Mg-BCP bioceramic stents sintered at 950 °C.

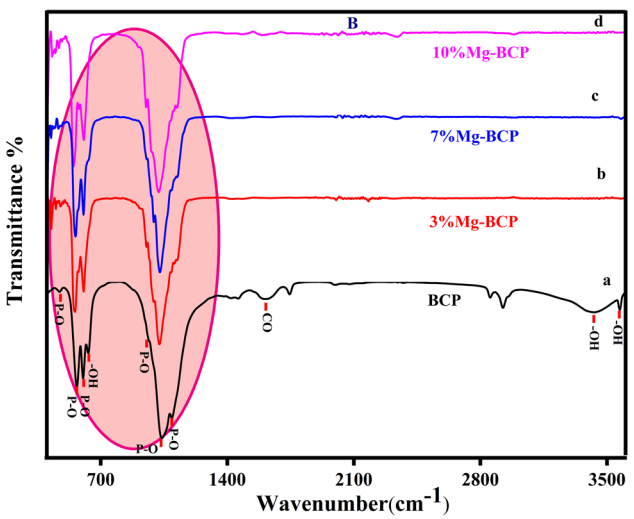

Fig. 3 FTIR spectra for pure BCP, 3%Mg-BCP, 7%Mg-BCP, and 10% Mg-BCP bioceramic stents.

Open Access Article. Published on 27 February 2023. Downloaded on 4/25/2026 11:50:07 AM.
This article is licensed under a Creative Commons Attribution-NonCommercial 3.0 Unported Licence.

vibrational motion of PO_4^{3-} molecules.[33] The asymmetric stretching vibration modes of the hydroxyl groups were observed at 3750 cm^{-1} and 631 cm^{-1} for the OH^- ion bending mode. Fig. 3(b)–(d) shows the minor changes in the respective phosphate ion absorbance and hydroxyl ion band intensity. Fig. 4 shows the HPO_4^{2-} and CO_3^{2-} absorption peaks at 885 cm^{-1} and 1422 cm^{-1}, respectively; however, the intensity of the HPO_4^{2-} and CO_3^{2-} bands is less than that of the PO_4^{3-} peak. The incorporation of Mg^{2+} ions resulted in a decrease in the peak absorbance intensity of the HPO_4^{2-} and CO_3^{2-} groups. The FTIR results indicated that the formed apatite is BCP, and that the β-TCP phase increased with increasing magnesium concentration; the XRD data in Fig. 2 also evidenced the increase in the β-TCP phase, as the β-TCP peak intensity increased compared to that in the graph of pure BCP XRD and no significant changes were noted.

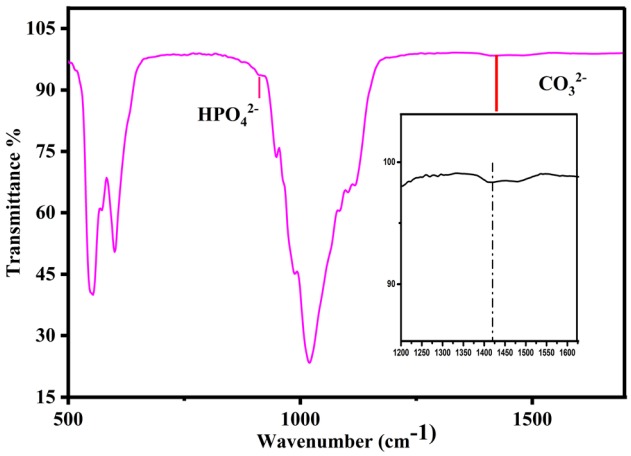

Fig. 4 FTIR spectra for 3%Mg-BCP and expansion of the peaks of HPO_4^{2-} and CO_3^{2-}.

FESEM analysis of fabricated small-diameter stents

The expected particle size and morphology of the small-caliber blood vessels fabricated using the synthesized pure biphasic calcium phosphate and biphasic calcium phosphate bioceramics with different percentages of magnesium ion doping are shown in Fig. 5. The FESEM image of the bioceramic tubular scaffold and the length of the porous scaffold, which was measured to be around 10 mm length, are shown in Fig. 5 (a and f). Fig. 5 (b)–(e) shows the FESEM observations of the synthesized magnesium-ion-doped biphasic calcium phosphate. The morphology exhibits a porous and agglomerated structure with interconnected particles, and average particle size was approximately 150 to 300 nm.[32]

Measurement of electrical properties using the EIS method

Blood conducts electrical signals because it contains salt and water as constituents. One of the main factors in the electrical conductivity of blood is the presence of sodium chloride ions. The only factor that influences the electrical conductivity of blood is the amount of water that is present in the fluid. The conductivity of water ranges from 0 to 500 μS cm^{-1}, whereas the average conductivity of blood is 10–20 mS cm^{-1}. These values conclusively show that water has a conductivity that is far higher than blood's. Measurements of electrochemical impedance in a medical-grade saline medium were performed to compare the electrical characteristics of the prepared vascular graft (sample size: 10 mm length) with human blood. Two intravenous maintenance fluids (0.45% and 0.9% of NaCl saline) were tested to check the conductivity of the developed vascular stent. Fig. 6 displays the conductivity determined for the bioceramic stent in both 0.45% and 0.9% NaCl solutions. In order to demonstrate that the 0.45% saline solution has a higher conductivity than the 0.9% saline solution, NaCl saline was calibrated as a baseline run. The conductance data have a nearly negligible offset from the NaCl observations. These results demonstrate that 0.45% NaCl saline is significantly more conductive than 0.9%

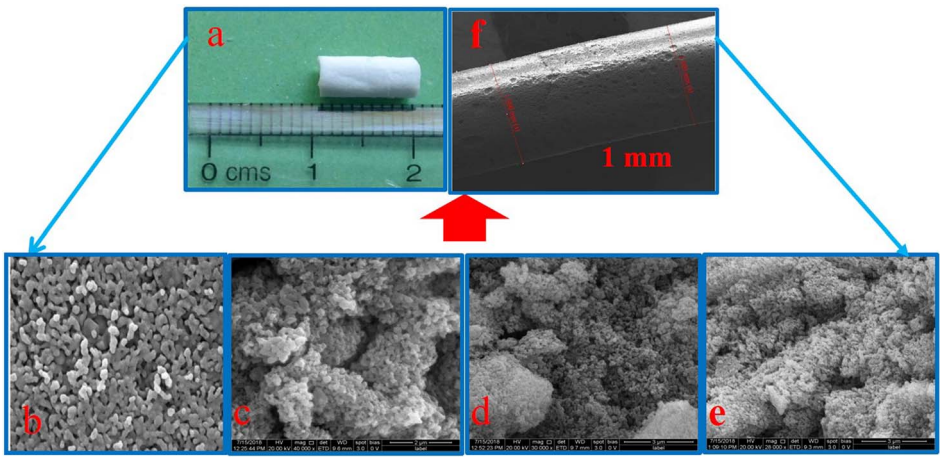

Fig. 5 Photographic image of the bioceramic stent (a) along with FESEM images for pure BCP (b) and various concentrations of Mg incorporated BCP (c). 3% Mg-BCP, (d) 7% Mg-BCP, and (e) 10% Mg-BCP. The (f) denotes FESEM micrograph of the bioceramic stent.

© 2023 The Author(s). Published by the Royal Society of Chemistry

Open Access Article. Published on 27 February 2023. Downloaded on 4/25/2026 11:50:07 AM.
This article is licensed under a Creative Commons Attribution-NonCommercial 3.0 Unported Licence.

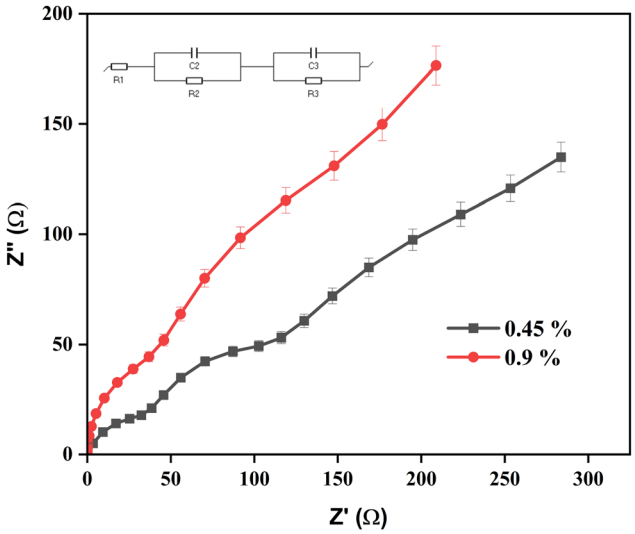

Fig. 6 Impedance spectroscopy for bioceramic stent (3%Mg-BCP). The data represent mean ± SD for triplicate experiments.

NaCl, with a charge transfer resistance (R_{ct}) of 78.31 ohm compared to 45.39 ohm for 0.9% NaCl. In this work, it was found that BCP with Mg^{2+} ions had electrical conductivity properties in both 0.45% and 0.9% NaCl saline solutions. As shown in Table 1, the obtained electrical parameters match the electrical characteristics of the biological components.[34,35] The 3%Mg-BCP bioceramic stent performed well in terms of its electrical characteristics, which is essential for cardiovascular applications.

In vitro analysis

Hemolysis. Analysis of hemocompatibility is crucial for determining the interactions of biomaterials with blood cells and bone matrixes. Estimation of hemolysis plays a vital role in the study of the biocompatibility of biomaterials and is an essential feature for *in vivo* applications. The small-caliber stents were evaluated for their non-hemolytic nature in contact with human blood cells, and all the samples were found to be hemocompatible according to the ASTM 756-00 and ISO 10993-5 1992 (American Society for Testing and Materials Designation) standards.[35,36] The *in vitro* hemocompatibility of pure BCP and biphasic calcium phosphate samples doped with various percentages of metal ions (Mg^{2+}) were measured, and the hemolysis percentages are presented in Fig. 7. Each sample was tested at four different concentrations (5, 10, 15, and 20 mg mL^{-1}) results were compared to positive control.

The results of the tests indicated that all samples exhibited a non-hemolytic nature, and the hemolysis percentages are presented in Table 2. The calculated hemolysis values were below 5% for all samples, with the exception of 10 mg of 7%Mg/BCP, which had a higher value than other concentrations of pure biphasic calcium phosphate and magnesium-ion-doped biphasic calcium phosphate.[30,37,38] Additionally, BCP with incorporated Mg^{2+} ions demonstrated a strongly non-hemolytic nature, although the hemolysis level for 7%Mg/BCP slightly increased above 5%, particularly at higher concentration levels. These results demonstrate the potential for the development of

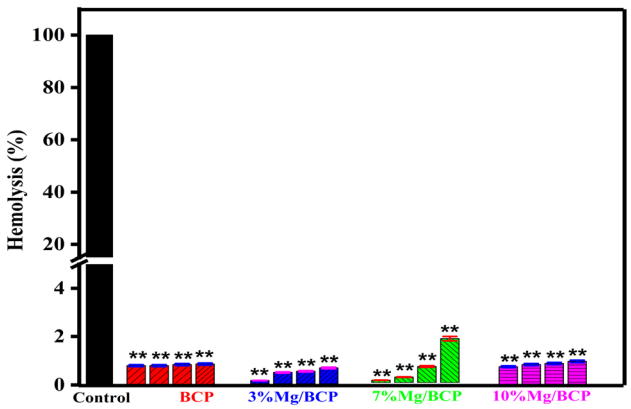

Fig. 7 Percentage hemolysis for pure BCP, 3%Mg/BCP, 7%Mg/BCP, and 10%Mg/BCP at the respective four concentrations. Data represent mean ± SD with triplicate biological experiments. $^{**}p < 0.01$ *vs.* positive control.

Table 2 Obtained hemolysis values for BCP, 3%Mg/BCP, 7%Mg/BCP, and 10%Mg/BCP bioceramic materials

S. No.	Sample code	Concentration (mg mL^{-1})	HR%
1	BCP	5	1.8
		10	1.8
		15	1.9
		20	1.95
2	3%Mg/BCP	5	0.31
		10	1.07
		15	1.18
		20	1.49
3	7%Mg/BCP	5	0.43
		10	0.90
		15	2.6
		20	7.0
4	10%Mg/BCP	5	1.7
		10	1.9
		15	2
		20	2.2

Table 1 Electrical resistivity data for the prepared material (3%Mg-BCP) and biological components

S. No.	Name of the component	Conductivity	Bioceramic stent	Electrolyte	Conductivity
1	Thoracic tissues	200–5000 ohm cm	3%Mg-BCP	0.45% NaCl saline	78.31 ohm
2	Blood and fluid	65–150 ohm cm	3%Mg-BCP	0.9% NaCl saline	45.39 ohm

Open Access Article. Published on 27 February 2023. Downloaded on 4/25/2026 11:50:07 AM. This article is licensed under a Creative Commons Attribution-NonCommercial 3.0 Unported Licence.

vascular stents that can be implanted into damaged blood vessels, as well as other types of conventional stents. According to the results, the samples are hemocompatible and should be safe for *in vivo* application.

Conclusion

In conclusion, the physico-chemical, electrical conductivity and hemocompatibility characteristics of synthesised pure BCP and 3%-, 7%-, and 10%-magnesium-doped biphasic calcium phosphate were examined for the fabrication of small-caliber stents through an extrusion technique. Furthermore, hemocompatibility measurements demonstrated that the magnesium-ion-doped BCP and pure BCP are both non-hemolytic, in nature, except the 7 mg concentration of 7%Mg/BCP. Finally, the results of *in vitro* hemolysis show that the prepared stents are suitable for cardiovascular prostheses.

Conflicts of interest

The authors declare no conflict of interest.

Acknowledgements

The authors acknowledge the financial support from the Indian Council of Medical Research (ICMR)-SRF No. 45/27/2019-NAN-BMS, TNSCST (TNSCST/S&T Projects/VR/MS/01/2016-2017), and DST-FIST and UGC-SAP are acknowledged for the instrumentation facilities.

References

1 X. Ren, Y. Feng, J. Guo, H. Wang, Q. Li, J. Yang, X. Hao, J. Lv, N. Ma and W. Li, Surface modification and endothelialization of biomaterials as potential scaffolds for vascular tissue engineering applications, *Chem. Soc. Rev.*, 2015, **44**(15), 5680–5742.

2 S. Borhani, S. Hassanajili, S. H. A. Tafti and S. Rabbani, Cardiovascular stents: overview, evolution, and next generation, *Prog. Biomater.*, 2018, **7**, 175–205.

3 Ju Hun Yeon, H. Ryu Ryu, M. Hwan Chung, Q. Ping Hu and N. Li Jeon, In vitro formation and characterization of a perfusable three-dimensional tubular capillary network in microfluidic devices, *Lab Chip*, 2012, **12**(16), 2815–2822.

4 J. Liu, J. Wang, Y.-f. Xue, T.-T. Chen, D.-n. Huang, Y.-x. Wang, K.-F. Ren, Y.-b. Wang, G.-s. Fu and J. Ji, Biodegradable Phosphorylcholine Copolymer for Cardiovascular Stent Coating, *J. Mater. Chem. B*, 2022, **8**(24), 5361–5368.

5 H. Nuhn, C. E. Blanco and T. A. Desai, Nanoengineered stent surface to reduce in-stent restenosis in vivo, *Appl. Mater. Interfaces*, 2017, **9**(23), 19677–19686.

6 W. S. Choi, Y. K. Joung, Y. Lee, J. W. Bae, H. K. Park, Y. H. Park, J.-C. Park and K. D. Park, Enhanced patency and endothelialization of small-caliber vascular grafts fabricated by co immobilization of heparin and vell-adhesive peptides, *Appl. Mater. Interfaces*, 2016, **8**, 4336–4346.

7 V. Montagna, J. Takahashi, M.-Yu Tsai, T. Ota, N. Zivic, S. Kawaguchi, T. Kato, M. Tanaka, H. Sardon and K. Fukushima, *Biomater. Sci. Eng.*, 2021, **7**, 472–481.

8 J. S. Lee, P. Han, E. Song, D. Kim, H. Lee, M. Labowsky, J. Taavitsainen, S. Yla-Herttuala, J. Hytönen, M. Gülcher, K. Perambalur, J. Sinusas, J. Martin, A. Mathur and T. M. Fahmy, Magnetically Coated Bioabsorbable Stents for Renormalization of Arterial Vessel Walls after Stent Implantation, *Nano Lett.*, 2018, **18**(1), 272–281.

9 R. Okner, Y. Shaulov, N. Tal, G. Favaro, A. J. Domb and D. Mandler, Electropolymerized Tricopolymer Based on N-Pyrrole Derivatives as a Primer Coating for Improving the Performance of a Drug-Eluting Stent, *Appl. Mater. Interfaces*, 2019, **1**(4), 758–767.

10 B. Oh and C. H. Lee, Advanced Cardiovascular Stent coated with Nanofiber, *Mol. Pharm.*, 2013, **10**(12), 4432–4442.

11 D. Son, J. Lee, D. Jun Lee, R. Ghaffari, S. Yun, S. Joo Kim, Ji Eun Lee, H. Rim Cho, S. Yoon, S. X. Yang, S. Lee, S. Qiao, D. Ling, S. Shin, J.-K. Song, J. Kim, T. Kim, H. Lee, J. Kim, M. Soh, N. Lee, C. Seong Hwang, S. Nam, N. Lu, T. Hyeon, S. Hong Choi and D.-H. Kim, Bioresorbable Electronic Stent Integrated with Therapeutic Nanoparticles for Endovascular Diseases, *Nano*, 2015, **9**(6), 5937–5946.

12 F. Rossi, T. Casalini, E. Raffa, M. Masi and G. Perale, Bioresorbable Polymer Coated Drug Eluting Stent: A Model Study, *Mol. Pharm.*, 2012, **9**, 1898–1910.

13 T. Ho Kim, Ji-H. Lee, C. Bum Ahn, J. Hee Hong, K. Hui Son and J. W. Lee, Development of a 3D-Printed Drug-Eluting Stent for Treating Obstructive Salivary Gland Disease, *Biomater. Sci. Eng.*, 2019, **5**, 3572–3581.

14 M. Santos, E. C. Filipe, P. L. Michael, J. Hung, S. G. Wise and M. M. Marcela Bilek, Mechanically Robust Plasma-Activated Interfaces Optimized for Vascular Stent Applications, *Appl. Mater. Interfaces*, 2016, **8**(15), 9635–9650.

15 L. Wang, Li Jiao, S. Shuo Pang, P. Yan, X. Wang and T. Qiu, The Development of Design and Manufacture Techniques for Bioresorbable Coronary Artery Stents, *Micromachines*, 2021, **12**, 990.

16 A. Fernández-Colino, F. Wolf, S. Rütten, T. Schmitz-Rode, J. Carlos Rodríguez-Cabello, S. Jockenhoevel and P. Mela, Small Caliber Compliant Vascular Grafts Based on Elastin-Like Recombinamers for in situ Tissue Engineering, *Front. Bioeng. Biotechnol.*, 2019, **7**, 340.

17 K. K. A. Mosas, A. R. Chandrasekar, A. Dasan, A. Pakseresht and D. Galusek, Recent Advancements in Materials and Coatings for Biomedical Implants, *Gels*, 2022, **8**(5), 323.

18 S. Prasadh, S. Raguraman, R. Wong and M. Gupta, Current Status and Outlook of Temporary Implants (Magnesium/Zinc) in Cardiovascular Applications, *Metals*, 2022, **12**, 999.

19 W. Li, Ya Su, L. Ma, S. Zhu, Y. Zheng and S. Guan, Sol-gel coating loaded with inhibitor on ZE21B Mg alloy for improving corrosion resistance and endothelialization aiming at potential cardiovascular application, *Colloids Surf., B*, 2021, **207**, 111993.

20 M. Moravej and D. Mantovani, Biodegradable Metals for Cardiovascular Stent Application: Interests and New Opportunities, *Int. J. Mol. Sci.*, 2011, **12**, 4250–4270.

© 2023 The Author(s). Published by the Royal Society of Chemistry

Open Access Article. Published on 27 February 2023. Downloaded on 4/25/2026 11:50:07 AM.
This article is licensed under a Creative Commons Attribution-NonCommercial 3.0 Unported Licence.

21 K. H. Bønaa, J. Mannsverk, R. Wiseth, L. Aaberge, Y. Myreng, O. Nygård, D. W. Nilsen, N.-E. Kløw, M. Uchto, T. Trovik, B. Bendz, S. Stavnes, R. Bjørnerheim, A.-I. Larsen, M. Slette, T. Steigen, O. J. Jakobsen, Ø. Bleie, E. Fossum, T. A. Hanssen, Ø. Dahl-Eriksen, I. Njølstad, K. Rasmussen, T. Wilsgaard and J. E. Nordrehaug, For the NORSTENT Investigators, Drug-Eluting or Bare-Metal Stents for Coronary Artery Disease, *N. Engl. J. Med.*, 2016, **375**, 1242–1252.

22 A. Santos-Coquillat, M. Esteban-Lucia, E. Martinez-Campos, M. Mohedano, R. Arrabal, C. Blawert, M. L. Zheludkevich and E. Matykina, PEO coatings design for Mg-Ca alloy for cardiovascular stent and bone regeneration applications, *Mater. Sci. Eng., C*, 2019, **105**, 110026.

23 J. Zong, Q. He, Y. Liu, M. Qiu, J. Wu and Bo Hu, Advances in the development of biodegradable coronary stents: A translational perspective, *Mater. Today Bio*, 2022, **16**, 100368.

24 M. Tavoni, M. Dapporto, A. Tampieri and S. Sprio, Bioactive Calcium Phosphate-Based Composites for Bone Regeneration, *Compost Sci.*, 2021, **5**, 227.

25 S. Basu and B. Basu, Unravelling Doped Biphasic Calcium Phosphate: Synthesis to Application, *Appl. Bio Mater.*, 2019, **2**(12), 5263–5297.

26 A. Jacobs, G. Renaudin, N. Charbonnel, J.-M. Nedelec, C. Forestier and S. Descamps, Copper-Doped Biphasic Calcium Phosphate Powders: Dopant Release, Cytotoxicity and Antibacterial Properties, *Materials*, 2021, **14**(9), 2393.

27 J. Jeong, J. Hun Kim, J. H. Shim, N. S. Hwang and C. Y. Heo, Bioactive calcium phosphate materials and applications in bone regeneration, Biomater, *Res*, 2019, **23**, 4.

28 J. Lu, H. Yu and C. Chen, Biological properties of calcium phosphate biomaterials for bone repair: a review, *RSC Adv.*, 2018, **8**, 2015–2033.

29 A. Marimuthu, M. Logesh and A. M. Ballamurugan, Zirconia Toughened BCP Bioceramic Material for the Fabrication of Small Diameter Blood Vessels for Cardiovascular Applications, *Trends Biomater. Artif. Organs*, 2021, **35**(1), 70–75.

30 M. V. B. dos Santos, L. B. N. Rocha, E. G. Vieira, A. L. Oliveira, A. O. Lobo, M. A. M. de Carvalho, J. A. Osajima and E. C. Silva-Filho, Development of Composite Scaffolds Based on Cerium Doped-Hydroxyapatite and Natural Gums—Biological and Mechanical Properties, *Materials*, 2019, **12**(15), 2389.

31 R. Fernández, C. Berruecos, M. C. C. Motta and D. Velásquez, Genotoxicity and Hemocompatibility of a Novel Calcium Aluminate-Based Cement, *Eur. Endod. J.*, 2018, **3**(2), 87–92.

32 I. Sopyan, T. A. rahim and Z. A. Ahmad, Magnesium-doped biphasic calcium phosphate nanopowders via sol-gel method, *Nova Sci Pub*, 2010.

33 S. Adzila, N. A. Mustaffa and N. Kanasan, Magnesium-doped calcium phosphate/sodium alginate biocomposite for bone implant application, *J. Australas. Ceram. Soc.*, 2020, **56**, 109–115.

34 W. H. Wilson Tang and W. Tong, Measuring impedance in congestive heart failure: current options and clinical applications, *Am. Heart J.*, 2009, **157**(3), 402–411.

35 G. S. Kassab, Electrical Conductance Device for Stent Sizing, Front, *Physiol*, 2019, **10**, 120.

36 M. Weber, H. Steinle, S. Golombek, L. Hans, C. Schlenk, H. P. Wendell and M. Avci-Adali, Blood-Contacting Biomaterials: In Vitro Evaluation of the Hemocompatibility, *Front. Bioeng. Biotechnol.*, 2018, **6**, 99.

37 (*a*) W. van Oeveren, Obstacles in Haemocompatibility Testing, *Scientifica*, 2013, **2013**, 392584; (*b*) R. FERNÁNDEZ, C. BERRUECOS, M. C. CORTÉS MOTTA and D. VELÁSQUEZ, Genotoxicity and Hemocompatibility of a Novel Calcium Aluminate-Based Cement, *Endod J.*, 2018, **2**, 87–92.

38 S. Braun, A. Lendlein and F. Jung, Developing standards and test protocols for testing the hemocompatibility of biomaterials, in *Hemocompatibility of biomaterials for clinical applications blood-biomaterials interactions applications blood-biomaterials interactions*, Woodhead Publ., 2018, pp. 51–76.

© 2023 The Author(s). Published by the Royal Society of Chemistry